X-661-70-106
PREPRINT

A LARGE AREA HIGH RESOLUTION COSMIC RAY CHARGE COMPOSITION DETECTOR

J. F. ORMES
V. K. BALASUBRAHMANYAN
R. D. PRICE
M. J. RYAN
R. F. SILVERBERG

MARCH 1970

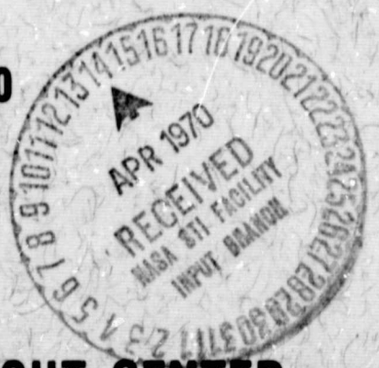

GODDARD SPACE FLIGHT CENTER
GREENBELT, MARYLAND

A LARGE AREA HIGH RESOLUTION COSMIC RAY CHARGE COMPOSITION DETECTOR

J. F. Ormes,* V. K. Balasubrahmanyan, R. D. Price
M. J. Ryan,+ and R. F. Silverberg#

NASA/Goddard Space Flight Center
Greenbelt, Md.

Abstract

A detector designed to study the charge composition of the primary cosmic radiation in the range Z = 3 to 30 has been flown on balloons during 1969. The flight is part of a program to study the charge composition in the energy range 10 to 10^5 GeV. The telescope consists of a four fold charge measurement using two plastic scintillators, a Cerenkov detector and a mosaic CsI (Na) detector. The intrinsic limitations on charge resolution due to statistical fluctuations in energy loss are approached by correcting the pulse heights for geometrical effects. This is accomplished by calibrating the detector response in flight using a spark chamber to determine the particle trajectories.

*Part of this work was done under a NASA-NRC Postdoctoral Resident Research Associateship.

+NASA-NRC Postdoctoral Resident Research Associate.

#University of Maryland

INTRODUCTION

Two years ago at this conference, (Ormes et al. 1968), an experiment designed to study the charge composition of the primary cosmic radiation in the energy range 10^{10} to 10^{14} ev from balloons and satellites was described. Since that time the experiment has been flown on a 10^{7} ft.^{3} balloon from Holloman Air Force Base in Alamogordo, New Mexico, where the vertical geomagnetic cutoff is 5 GV. It reached an altitude of 107,000 ft. where it floated for 15 hours. The equipment was recovered near Houston, Texas the next day after a 30 hour flight. We wish to present here some of the details regarding the operation of the charge detection section.

To place this report with respect to the overall program objectives, a brief review is appropriate. The low energy charge composition has been thoroughly studied but essentially no direct information is available above 20 GeV/nucleon. Recent work on the origin and propagation of the cosmic radiation (e.g., see Ramaty and Reames, 1970) suggests that many of the open questions may be answered by studies at higher energies. An implication of their work is that the charge composition may vary with energy and that an anisotropy may be present for heavier nuclei. Detailed charge composition information must be obtained as a function of energy in order to answer these questions.

For example, the nuclei in the charge range Z = 20-25 are believed to be produced mostly by spallation reactions of iron in its passage through interstellar matter (Lezniak et al. 1969). An accurate measure-

ment of the relative fluxes in this charge range can lead to an estimate of the mean amount of matter traversed by the iron nuclei. This estimate can be then compared to that obtained from the production of Li, Be, and B nuclei from spallation of the carbon and oxygen. This specific problem requires resolution of $\pm 1/2$ a charge in the iron region.

In Figure 1, the complete instrument is schematically illustrated. At the top is the charge determination section, consisting of two plastic scintillators, a lucite Cerenkov radiator, and a CsI mosaic scintillator, each 50 cm x 50 cm. These four detectors provide response proportional to square of the particle charge. Included in this section are four wire grid spark chambers (Ehrmann et al. 1967) for determining the direction and the position of the particle passing through the instrument. Beneath this is an electron cascade section for measuring the electron spectrum and an ionization spectrometer for determining the energy of the particle. This electron section has been flown and calibrated at the Stanford Linear Accelerator Center and will be discussed elsewhere. The operation and properties of ionization spectrometers have been described in detail elsewhere (e.g., see Murzin, 1965, Jones, et al. 1969, or Grigorov et al. 1958) and will not be discussed here.

In April the instrument will be flown from a balloon with an ionization spectrometer. This is the first step in a series of measurements which will determine the charge spectrum as a function of energy.

It is hoped the series will culminate in a satellite flight for it is only with the long exposures that a statistically significant number of heavy nuclei can be collected at 10^{12}-10^{14} eV.

CHARGE RESOLUTION

The ability to separate adjacent charges is determined by three main factors:

a. The intrinsic statistical fluctuations in energy loss in the detector and the subsequent conversion of that energy to light,

b. photo electron statistics, and

c. all the geometrical effects which produce variations in the light produced and collected.

In this paper the intrinsic limitations on resolution will be discussed first. Secondly the size of and the corrections for various geometrical effects will be investigated. Also some discussion of the application of the large area Cerenkov detector will be given.

Since the aim is to determine charge within $\pm 1/2$ a charge up to and including Fe (Z = 26) resolution of $\pm 4\%$ is required. The difficulty of this task is illustrated by the corrections to be outlined in the following work. It is possible that an intrinsic limit may exist.

In Figure 2 a summary of the intrinsic resolutions involved is presented. The dashed line represents the separation between charges and the points represent full widths at half maximum (FWHM) calculated from the Landau distributions for a single detector. Note that at

8.4 GeV (near the mean energy of response for a balloon flight conducted where the cutoff is 1.75 GeV/nuc) the FWHM exceeds the separation for Z > 22. At high energies the problems extend well down to Z = 16. This is further worsened by the skewness of the distribution becoming more extreme at higher energies. This is shown in Table 1 where the probability of a Z of 25 simulating the ionization of other charges is given. (For reference purposes, the energy lost by an Fe of these energies is about 1.3 GeV in a 1/4" plastic scintillator.) This table illustrates that while the FWHM does not get worse at higher energies the distribution becomes more skew making possible an error of 1, 2 or even more charges.

It would appear from this table that our goal is completely unachievable above a few GeV/nuc. However, the situation is not as bad as it seems at first because the fluctuations which cause the skewness of the Landau distribution are caused by the production of a few very high energy knock-on electrons. Since these knock-on electrons have sufficient range to carry their energy out of the detector, the distribution of light produced will not exhibit this extreme skewness. The tail from the distributions are effectively removed and the problem of fluctuations exhibited in Table 1 is greatly reduced. However, this gives rise to another effect. Then a significant fraction of the energy lost goes into electrons which leave the detector so that the mean light output is reduced. The last column in Table 1 shows this effect becomes important for iron at energies above 25 GeV.

Because any single measurement of charge is subject to these statistical fluctuations, multiple measurements are essential. This is why four separate measurements of the charge have been deemed necessary. Extreme fluctuations will appear as an anomalous pulse height value in only one of the four detectors, greatly reducing its effect.

Once energy and charge measurements become available simultaneously it should be possible to study these effects. At any rate, because one wishes to operate at the limit of the intrinsic resolutions, the variations in pulse height due to systematic effects must be reduced to a few percent.

GEOMETRICAL EFFECTS

Because of the extremely low fluxes involved, a large geometric collection area must be used in order to measure a statistically significant number of particles. This can be achieved both by using large area detectors and by small separation of the geometry defining elements. In our case, 2700 cm^2 ster has been achieved using 50 cm x 50 cm geometry defining elements 30 cm apart. This small separation means that particles can traverse the detector at path lengths up to 2.2 x the minimum path length. This is illustrated in Figure 3 which shows the differential geometry as a function of path length in the detectors. Most path lengths are near the minimum but the long tail is extremely troublesome when trying to separate a rare charge from an adjacent abundant one.

A spark chamber has been used to calibrate the response for the geometrical effects. Its operation is considered briefly.

a. Spark Chamber. The technique of combining spark chambers with charge devices for better resolution using larger areas is relatively new. The group at the Danish Institute has reported its use in studying the cosmic rays up to the 1 GeV range (Corydon-Petersen, et al. 1969).

In this application the particle trajectories are determined using four pairs of perpendicularly oriented wire grid planes. The position of the trajectory is stored until readout in magnetic cores at the ends of the wires. There are 200 wires spanning the 50 cm detector length separated by 0.1 in.

Because the detector must be sensitive to electrons and iron nuclei, the spark chambers are being required to operate over a very large dynamic range in dE/dx (almost 10^3). In addition they must operate in the presence of all the knock-on electrons produced by high Z, high energy, particles. The spark chambers are operated at the knee in the efficiency voltage curve, about 2750 volts. This yields an efficiency of $\approx$ 98% for singly charged minimum ionizing particles, the sea level muons. At this voltage between 1.5 and 2 wires were set per spark. During the flight this spark spreading was found to increase with Z up to about 3 at Z = 3. Unfortunately at these large values of spreading an electronic inefficiency developes in the ability to read out the set cores and so it is not possible to measure the spreading at higher Z values. This inefficiency results

in unset cores within bunches of set cores and confuses the exact location of the track. In addition, the knock-on electrons which produce satellite tracks, increase like the square of the charge. At 1.5 GeV/nuc. approximately 7% of energy lost by a particle in crossing the spark chamber goes into electrons with sufficient range to cross all four grids.

Because of the large scattering suffered by these low energy electrons, they tend to random walk away from the trajectory and produce extraneous breakdowns.

The net result of these effects is that as Z increases, an inefficiency developes in the ability of the algoritims developed for computer analysis to determine the trajectory. This inefficiency, while greatly complicating the data analysis, can be determined and so correct fluxes can be derived.

A spark chamber track for a carbon nucleus is illustrated in Figure 4. The chamber is separated into an x, z view (upper 4 lines) and a y, z view. Every 5th wire is shown as a dot and each set core is denoted by a verticle line.

Because of these difficulties with one spark chamber one must convince oneself that the detector is giving trajectories correct to within a few degrees. If satisfactory, then the trajectories can be used to make corrections of up to 200% to the pulse height values with confidence. In Figure 5, we have plotted a histogram of numbers of

particles at various zenith angles. This can be seen to agree quite closely with the differential geometry as a function of zenith angle, except possibly for a slight absence of particles at large zenith angles. This slight deficit, if in fact real, can be understood in terms of the increased atmospheric absorption of carbon at larger angles. This good agreement indicates that the trajectories must be accurate to within a few degrees.

b. Zenith Angle Corrections. Since all of the detectors respond proportionately to the path length, this effect represents the largest correction which must be made. Even in the range of charges carbon, nitrogen and oxygen, the most plentiful of the cosmic ray heavy nuclei, carbon at $\sec\theta \geq 1.55$ looks like oxygen and between $\sec\theta = 1.2$ and 1.55 looks like nitrogen. In the range Z = 20 to 30, a charge 20 can look like a charge 28.

The $\sec\theta$ correction is checked using carbon nuclei because they are the most plentiful and because they lie in the range of amplification where no nonlinear effects are present. Since this correction ought to be proportional to $\sec\theta$, all pulse height values are corrected by this amount. The resultant charge resolution is quite adequate for identifying the carbon nuclei on two dimensional histograms. Pulse heights from the four detectors are then selected to include only carbon nuclei, and a two dimensional histogram is made of the response of the detectors (uncorrected) as one variable and zenith angle as the other. All these data points are then fed to a computer program which

finds a polynomial is weighted by the number of events at a given angle so the curve should be most accurate between 15 and 45^{o}.

The data is shown in Figure 6 for the four detectors. As can be seen from this figure, secθ is a good representation (within 2%) for the two plastic scintillators S1 and S2. A previously reported deviation (Ormes and Balasubrahmanyan, 1969) has subsequently been found to be due to analyzer non-linearities.

In the case of CsI the agreement is not good beyond 40^{o}. This discrepancy can be understood in the following manner. The CsI scintillator is placed in a box painted white with photomultipliers at the four corners. The tubes face the white surface opposite the CsI and there are no direct paths for light to follow from the scintillators into the photocathodes. However, light which comes from a spot near the tubes is collected more efficiently than light from the center. In fact when the detector is divided into nine squares, the center square if found to produce about 15% less signal than the average from the other areas. This affects the response as a function of zenith angle because extreme trajectories cannot pass through the central region. The enhancement at large zenith angles is due to trajectories which come nearer to photomultipliers and thus produce larger light pulses. The less extreme trajectories are distributed much more equally across the area of the detector. Understanding the cross coupling of two separate geometric effects such as these is sometimes quite difficult.

c. Positional variations. Variations in response of the S1 scintillator have been studied as a function of position. The detector is viewed by photomultiplier tubes through adiabatic light guides attached to two opposite edges, defined here as the y = 0 and y = 50 cm ends. Light striking the two open edges will either be lost or totally internally reflected. The light collection efficiency F(x,y) is in general a function of two variables.

$$F(x,y) = g(x)h(y)f(x,y)$$

It can be expressed as the product of a separable part g(x)h(y) and an inseparable part f(x,y).

In Figure 7 the relative responses as functions of position are plotted as percentage deviations from the mean. The function h(y) varies systematically from -3% near the edges to +3% in the middle. The function g(x) is constant within errors. Since the variations in F(x,y) are somewhat larger than those of g(x) and h(y), f(x,y) must be comparable to or greater than g and h in certain localized spots. The most extreme case is the lower right hand corner which seems to be 6 or 7% below average.

The variation in y position is quite symmetrical reflecting good balance in the gain of the two photomultiplier tubes. This variation with a peak at the center is consistent with the shape of the attenuation curves for Pilot B (Walker, 1969). However the amplitude of this variation is larger, probably due to the different geometry.

The responses of the three scintillators have been found to be independent of the azimuthal angle of the incident particles to within ±2%. This is consistent with the isotropic nature of the scintillation light production process. Any variation of this sort in the CsI response could have been attributed to an imbalance in the gains of photomultiplier tubes at the four corners.

d. Cerenkov. The Cerenkov response as a function of zenith angle is shown in Figure 6. Also shown is the calculated response based upon the fraction of the light which is totally internally reflected (Jelly, 1958). The response varies much more strongly than predicted. This is not yet understood. The 1/2" thick Lucite radiator is being viewed through all four edges by adiabatic light guides. The outputs of the four photomultipliers are then summed. Minimum ionizing particles are producing between 1 and 2 photo-electrons. Once the measured zenith angle variations are corrected the resolution is found to contain a FWHM of $\approx$ 30% due to other geometric effects. This means that even at carbon photo-electron statistics still dominate the resolution. Azimuthal variations reflecting imbalance of the photomultipliers (obviously very difficult to balance using muons) are ±9%. It is possible that the variations with area which have not yet been successfully determined are large and coupled with the zenith angle variations.

At this point it is not possible to use the Cerenkov for accurate charge measurements, but it does provide a useful consistency check on the scintillation measurements. It has also been very useful in rejecting

low energy background which is copious at our depth of 7 gm/cm^2 in the atmosphere.

CONCLUSION

A charge histogram which results from this analysis is shown in Figure 8 taken from a two dimensional distribution of S_1 vs CsI. This data includes only the zenith angle corrections. Unfortunately an amplifier saturation problem at about Z = 22 confuses the CsI response in the high Z region and so the goal of $\pm 1/2$ a charge has not really been adequately tested. However, it looks as though variations of a few percent can be calibrated, especially in those cases where the appropriate variable can be determined. Once this has been completed, it should be possible to decide whether an intrinsic charge resolution limitation exists or not at these energies.

REFERENCES

1. Corydon-Petersen, O., Dayton, B., Lund, N., Melgaard, K., Omø, K., Peters, B., and Risbo, T., "Design and Performance of an Instrument for Determining the Chemical Composition of Primary Cosmic Radiation" and Corydon-Petersen, O., and Lund, N., "Cosmic Radiation Experiment", Danish Space Research Institute Lundtoftevej 7, 2800 Lyngby, Denmark (to be published in the Proceedings of the 11th International Conference on Cosmic Rays, Budapest, Hungary, 1969).

2. Ehrmann, C.H., Fichtel, C.E., Kniffen, D.A., and Ross, R.W., "A Magnetic Core Digitized Spark Chamber for Space Science Experiments", Goddard Report, X-611-67-267.

3. Grigorov, N.L., Murzin, V., and Rapoport, I., Soviet Phys., J.E.T.P., 7, 348, 1958.

4. Jelly, J.V., "Cerenkov Radiation=and its Applications", Pergamom Press, 1958.

REFERENCES (Continued)

5. Jones, W.V., Pinkau, K., Pollvogt, U., and Schmidt, W.K.H., Inst. and Methods, 72, 173, 1969.

6. Lezniak, J.A., von Rosenvinge, T.T., and Webber, W.R., "The Chemical Composition and Energy Spectra of Cosmic Ray Nuclei with Z = 3 - 30" (to be published in the Proceedings of the 11th International Conference on Cosmic Rays, Budapest, Hungary 1969).

7. Murzin, V.S., "The Ionization Calorimeter", Progress In Cosmic Ray Research, Vol. 9, Chapter IV, 247, 1965.

8. Ormes, J.F., Balasubrahmanyan, V.K., McDonald, F.B., and Price, R.D. "A Method of Measuring the Cosmic Ray Charge Composition between 10^{10} and 10^{14} eV", IEEE Transactions on Nuclear Science, Vol. NS-15, June 1968, 566.

9. Ormes, J.F., and Balasubrahmanyan, V.K., "High Energy Program of Goddard Space Flight Center", (to be published in the Proceedings of the 11th International Conference on Cosmic Rays, Budapest, Hungary, 1969).

10. Ramaty, R., Reames, D.V., and Lingenfelter, R.E., "Statistical Discrete-Source Model of Local Cosmic Rays" (to be published in the Physical Review, 1970, and references therein).

11. Walker, J.K., Nuc. Inst. and Methods, 68, 131, 1969.

Figure 1. A schematic drawing of the experiment. The charge identification section at the top contains the two plastic scintillators which define the geometry, the CsI scintillator viewed by four PM tubes at the corners of a white light diffusion chamber, and the Cerenkov counter viewed through the four edges through adiabatic light guides. This section also contains four spark chamber grids for determining the trajectories of particles through the apparatus. The second section is a Tungsten scintillator sandwich primarily for electron measurements. The bottom section is the ionization spectrometer for measuring the energy of the nucleonic components. It consists of iron with scintillator slabs every 1.5 radiation lengths.

Figure 2. The intrinsic resolution due to Landau statistical fluctuations in energy loss as a function of Z (solid curves) compared with the resolution required to separate adjacent charges.

Figure 3. The differential geometry as a function of path length through the detector.

Figure 4. A spark chamber trajectory for a carbon nucleus. Note the satellite sparks near the trajectory which are presumably due to knock-on electrons. This figure is from a slide taken of a 2250 graphics display unit which can be used to look at individual events. The pulse height values for the 16 detectors are given at the top in convenient representations.

Figure 5. Comparison of the zenith angle distribution of detected carbon nuclei compared with the differential geometry as a function of zenith angle.

Figure 6. Response of the four charge detectors as a function of path length through the telescope. The data are compared with calculated responses. Note that the scale for the Cerenkov response curve on the right hand side is different from the other three.

Figure 7. Percentage variations from the mean response as a function of position and of the linear dimensions of the S1 plastic scintillator.

Figure 8. Charge histograms from balloon flight data.

TABLE 1

Some Statistics on Landau Distributions for Relativistic Iron Nuclei

Energy (GeV/nuc)	$\gamma = \frac{E}{mc^2}$	E_t(MeV)*	P(< 24.5)	P(> 25.5)	P(25.5 - 26.5)	P(26.5 - 27.5)	P(> 27.5)	f_{out}**
5.7	7.1	10	.03	.13	.02	0	0	0.8%
8.44	10	10^2	.01	.26	.10	.01	0	3.5%
28.7	31.4	10^3	.12	.52	.31	.14	.07	10.4%
93	100	10^4	.12	.57	.37	.22	.15	15.5%

* E_t is the maximum energy which can be transferred to a single knock-on electron.

** f_{out} is the fraction of energy into electrons with range greater than the detector thickness.

FIGURE 1

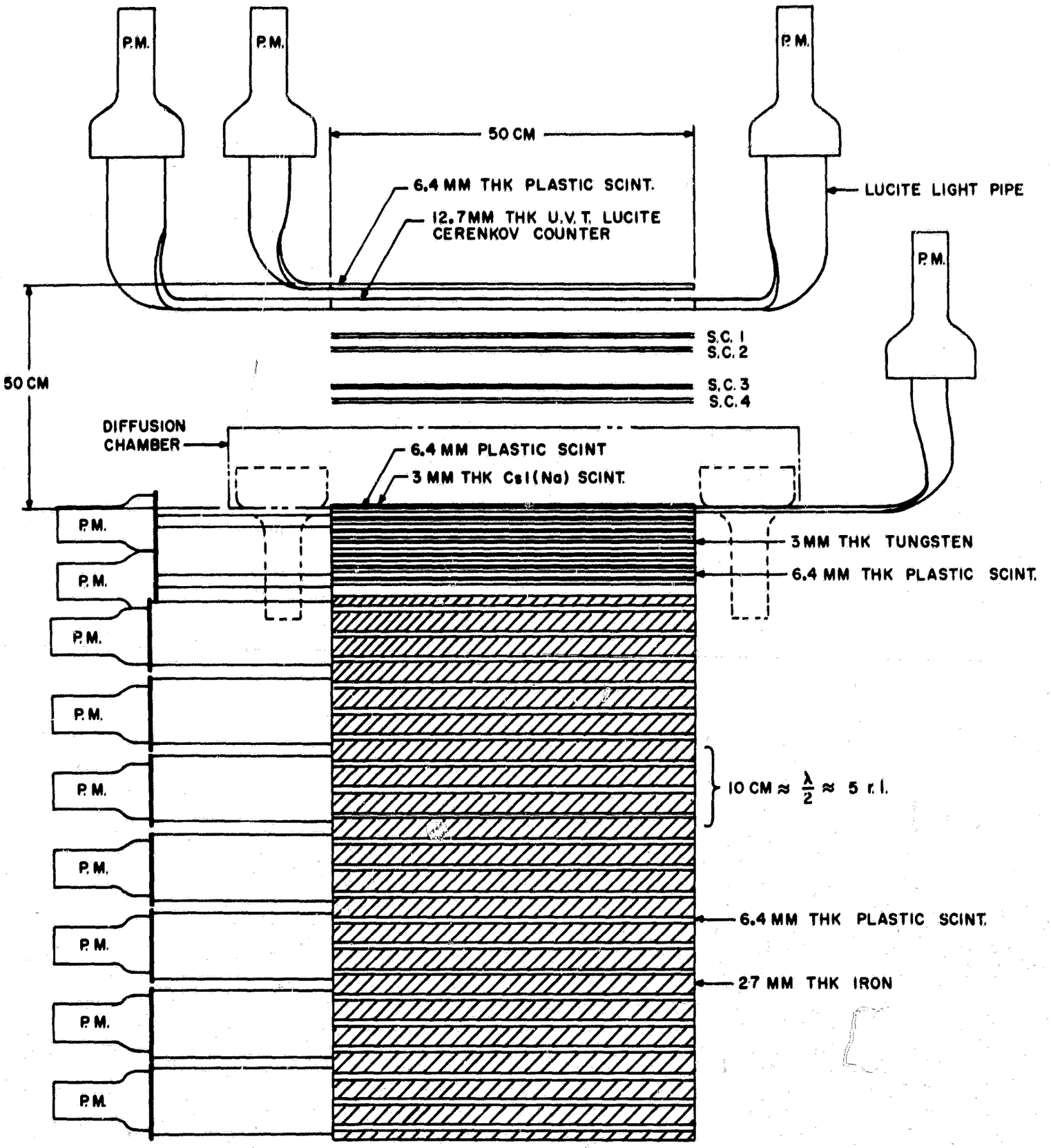

IONIZATION CALORIMETER

FIGURE 2

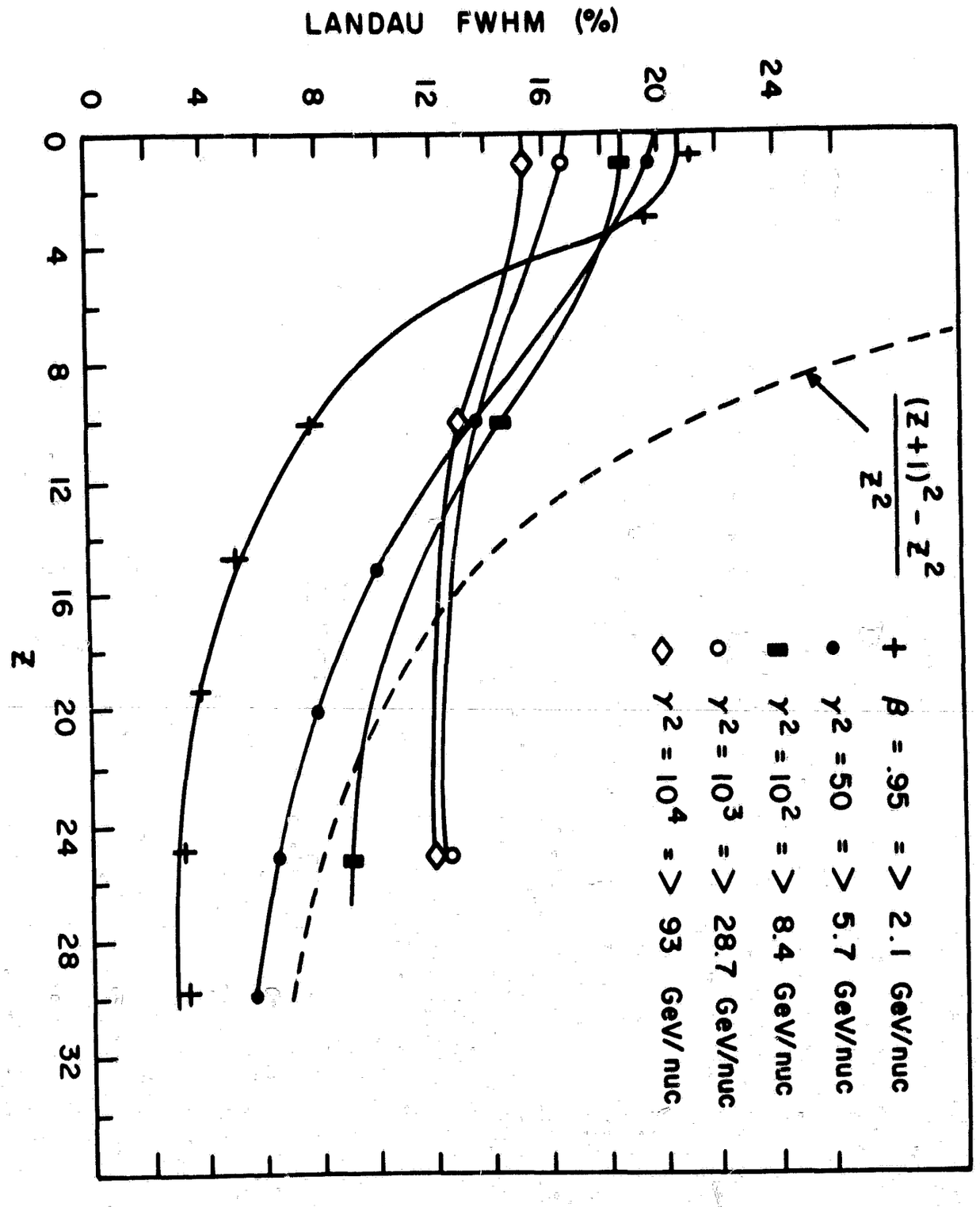
LANDAU FWHM (%)
0
4
8
12
16
20
24
Z
0
4
8
12
16
20
24
28
32
$\frac{(Z+1)^2 - Z^2}{Z^2}$
+ β = .95 => 2.1 GeV/nuc
• γ2 = 50 => 5.7 GeV/nuc
■ γ2 = 10^2 => 8.4 GeV/nuc
○ γ2 = 10^3 => 28.7 GeV/nuc
◇ γ2 = 10^4 => 93 GeV/nuc

FIGURE 3

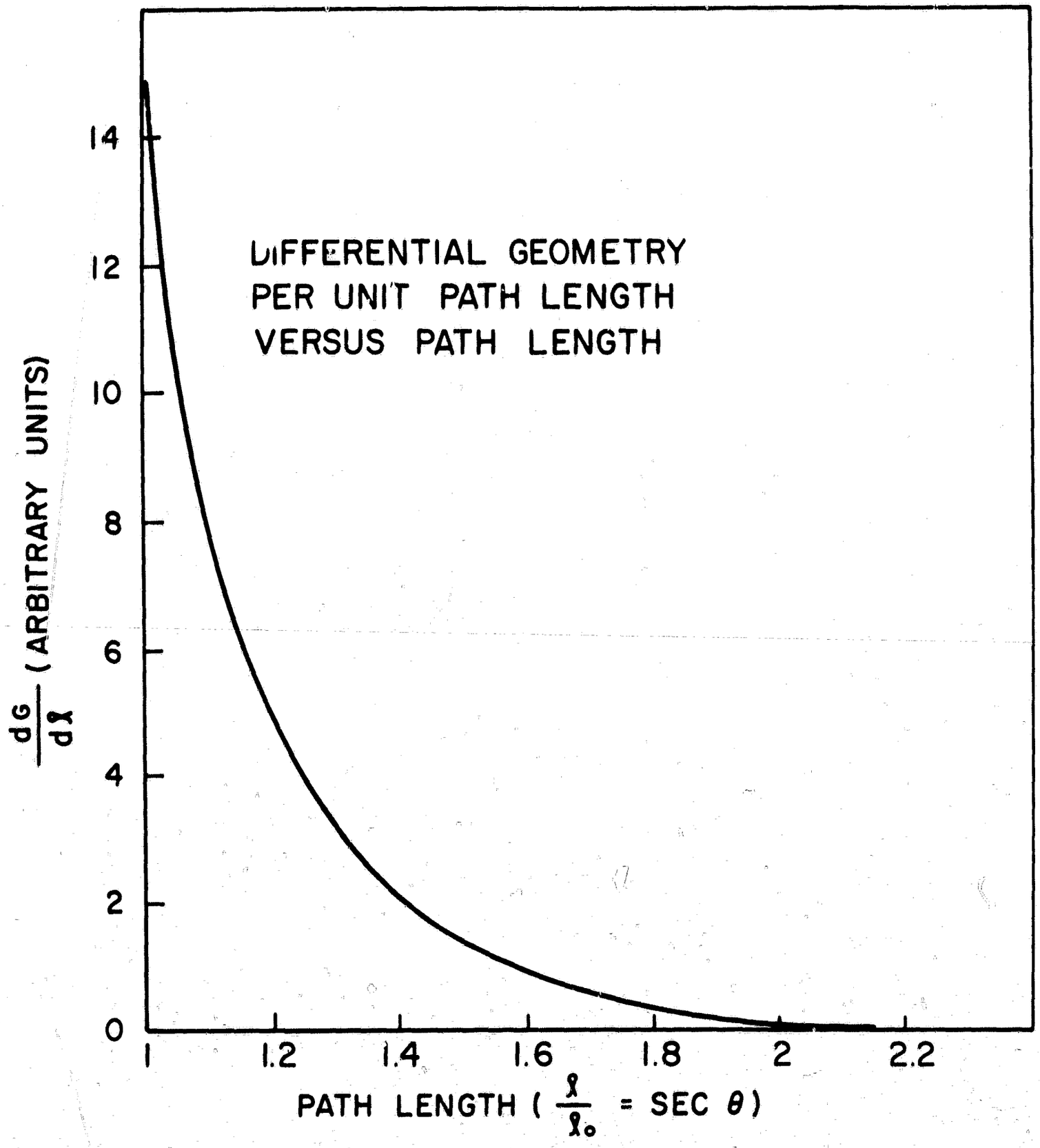
DIFFERENTIAL GEOMETRY
PER UNIT PATH LENGTH
VERSUS PATH LENGTH
$\frac{dG}{d\ell}$ (ARBITRARY UNITS)
0
2
4
6
8
10
12
14
1
1.2
1.4
1.6
1.8
2
2.2
PATH LENGTH ($\frac{\ell}{\ell_0}$ = SEC θ)

```
16 PH VALUES (UNCORRECTED)
 336 324 311  74 314 339 324 324   0   0   0   0   0   0   0   0
16 PH VALUES (CORRECTED)
 328 317 310  67 309 332 318 318   0   0   0   0   0   0   0   0

EVENT NO. =        0      THETA =  2.34989E+01     ALPHA =  1.65340E+02
```

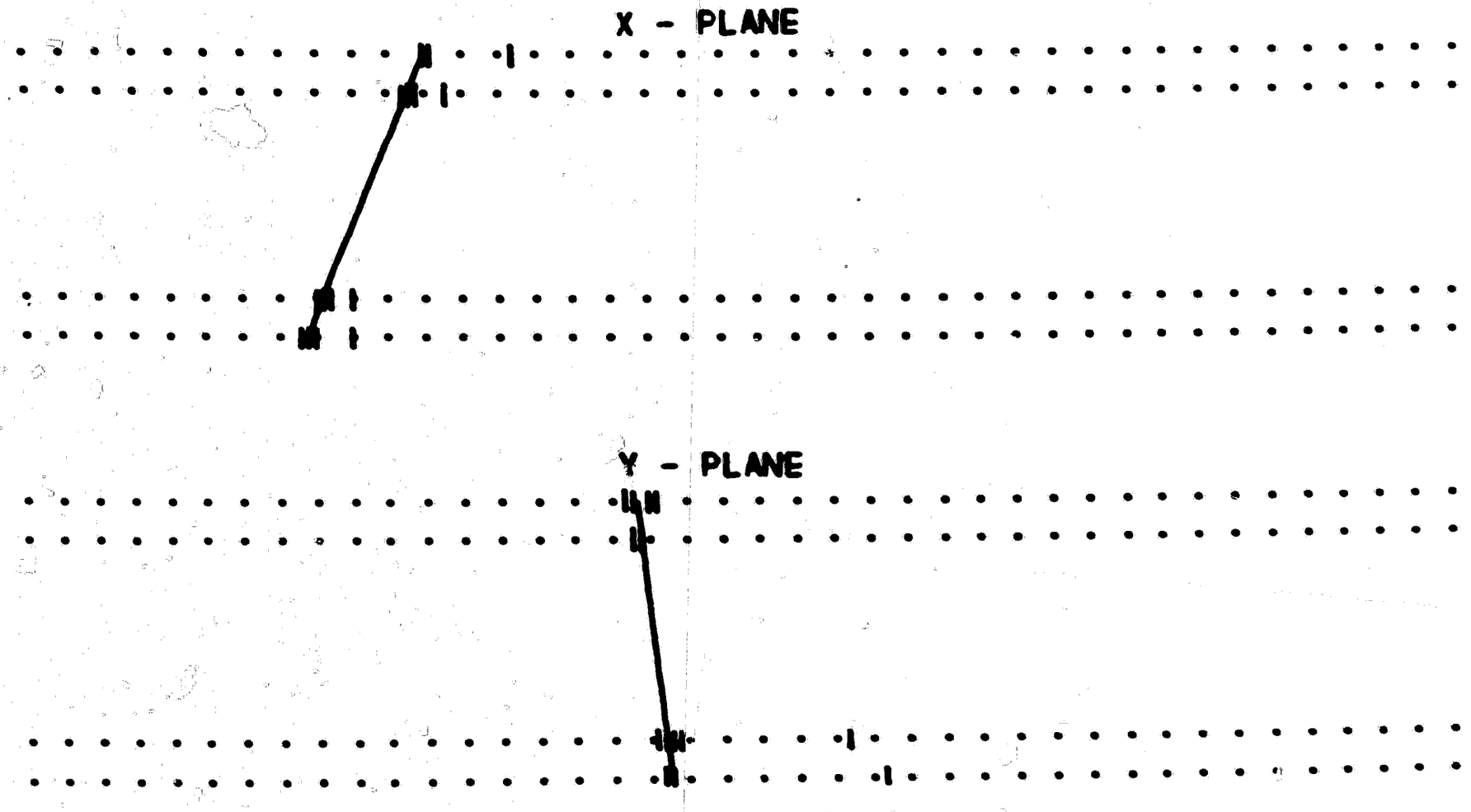


```
ERRX =  3.11053E-02     ERRY =  4.34551E-02
OPTIONS:
 RECALCULATE TRAJECTORY     X     Y
 SAVE EVENT    OLD    NEW
 PROCESS NEXT EVENT
 TERMINATE JOB
```

FIGURE 4

FIGURE 5

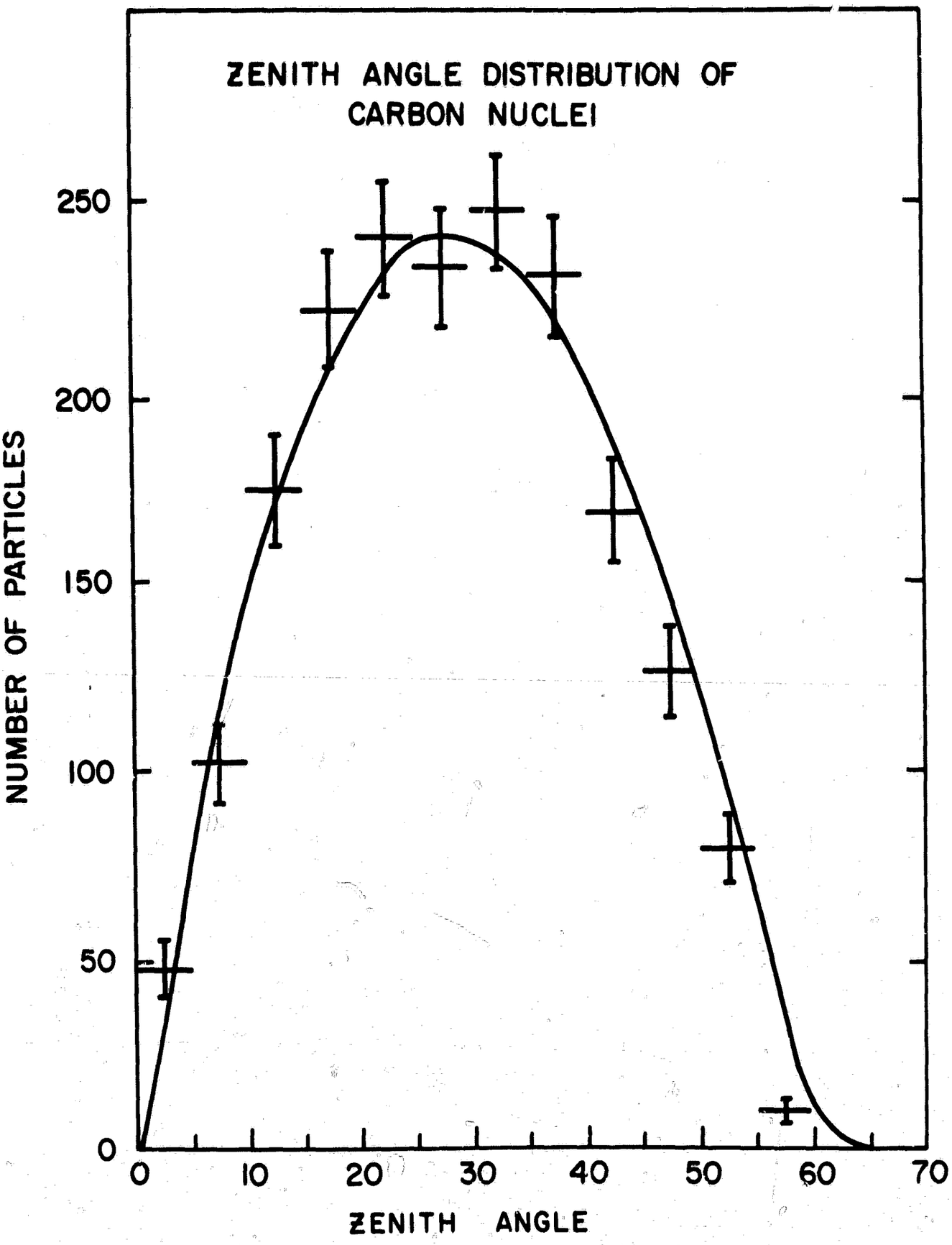
ZENITH ANGLE DISTRIBUTION OF
CARBON NUCLEI
NUMBER OF PARTICLES
250
200
150
100
50
0
0
10
20
30
40
50
60
70
ZENITH ANGLE

FIGURE 6

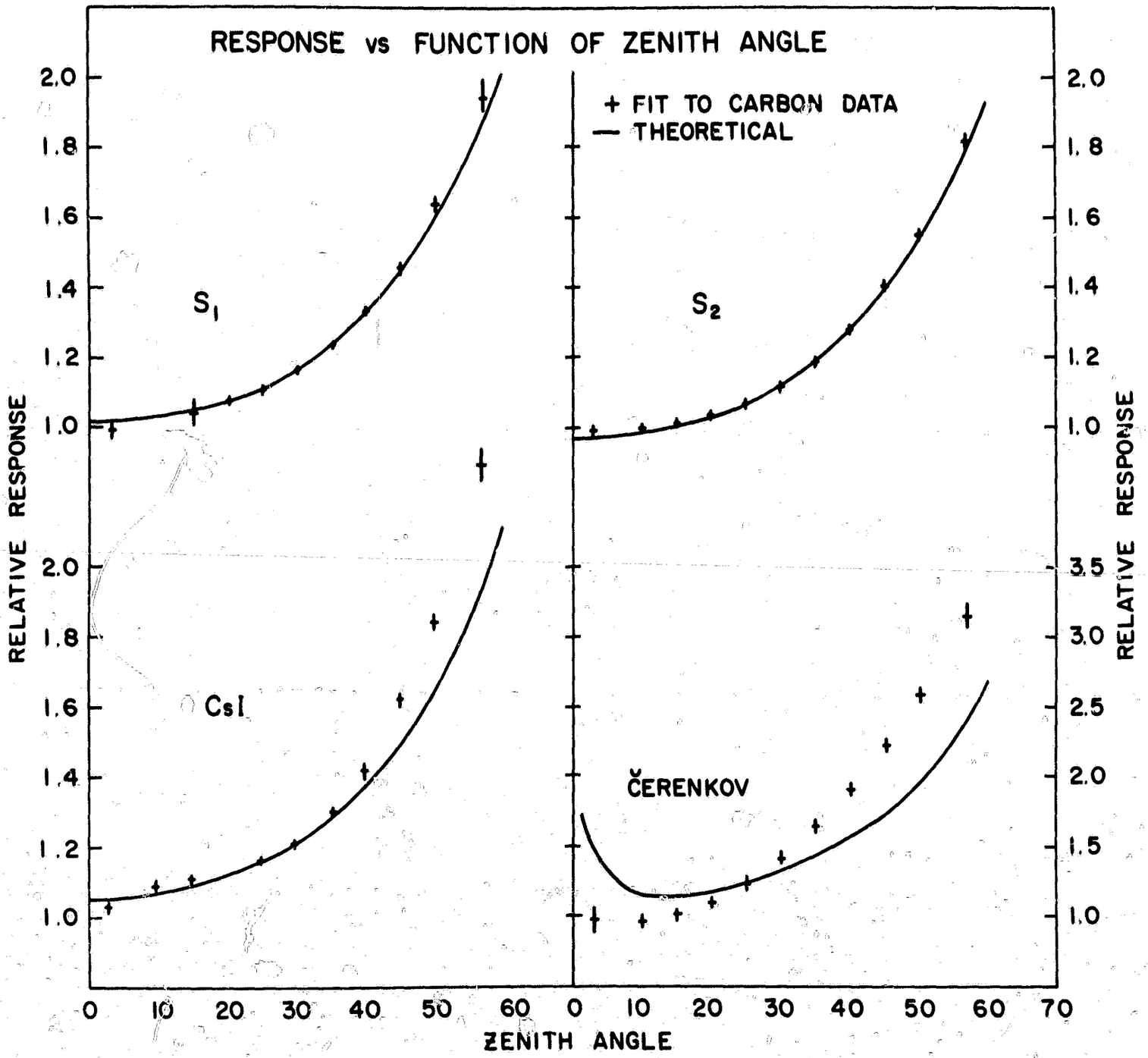
RESPONSE vs FUNCTION OF ZENITH ANGLE
+ FIT TO CARBON DATA
— THEORETICAL
S1
S2
CsI
ČERENKOV
RELATIVE RESPONSE
RELATIVE RESPONSE
ZENITH ANGLE
2.0
1.8
1.6
1.4
1.2
1.0
3.5
3.0
2.5
2.0
1.5
1.0
0
10
20
30
40
50
60
70

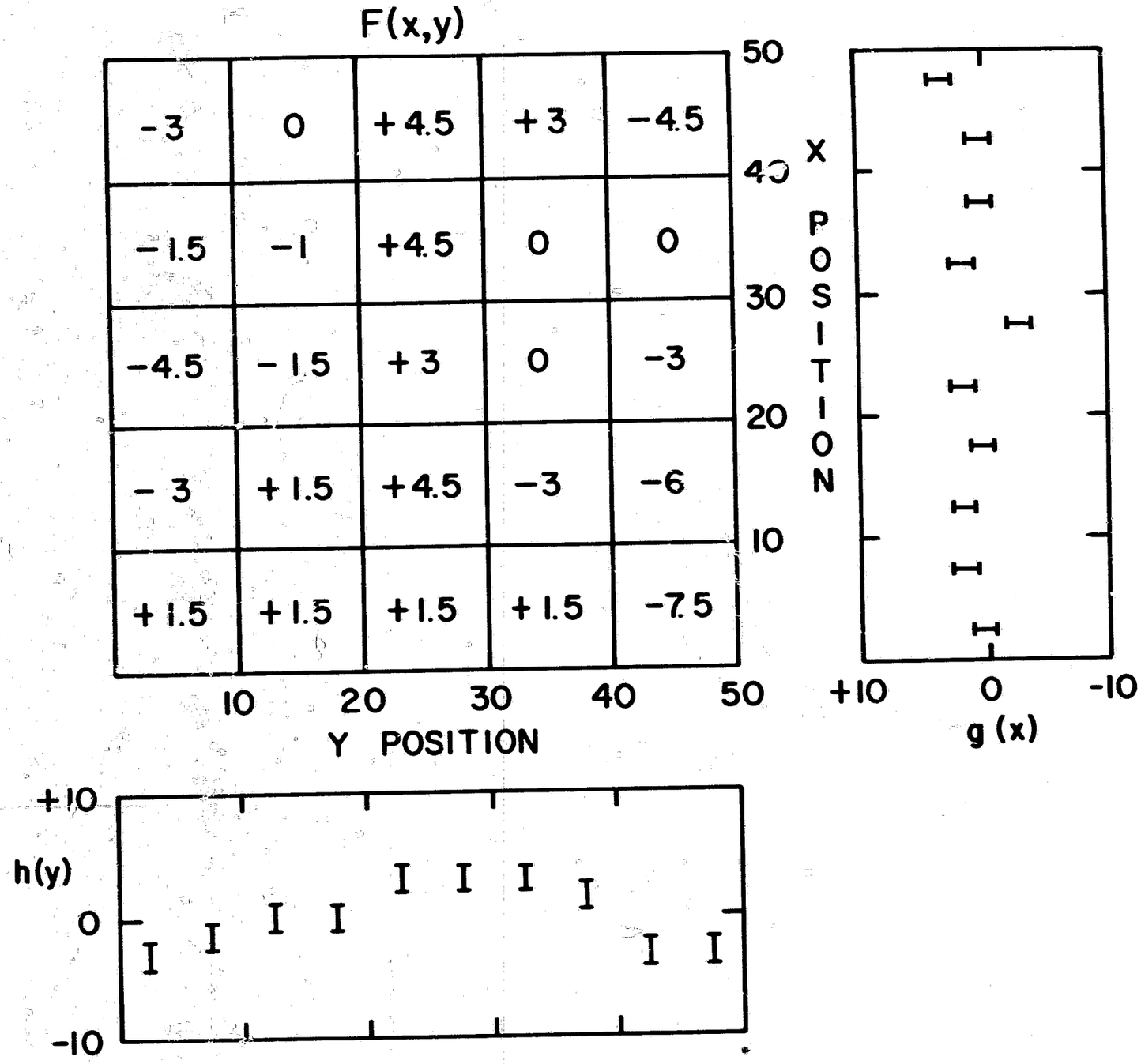
F(x,y)
-3 0 +4.5 +3 -4.5
-1.5 -1 +4.5 0 0
-4.5 -1.5 +3 0 -3
-3 +1.5 +4.5 -3 -6
+1.5 +1.5 +1.5 +1.5 -7.5
50
40
30
20
10
10 20 30 40 50
Y POSITION
X POSITION
+10 0 -10
g (x)
+10
h(y)
0
-10

FIGURE 7

FIGURE 8

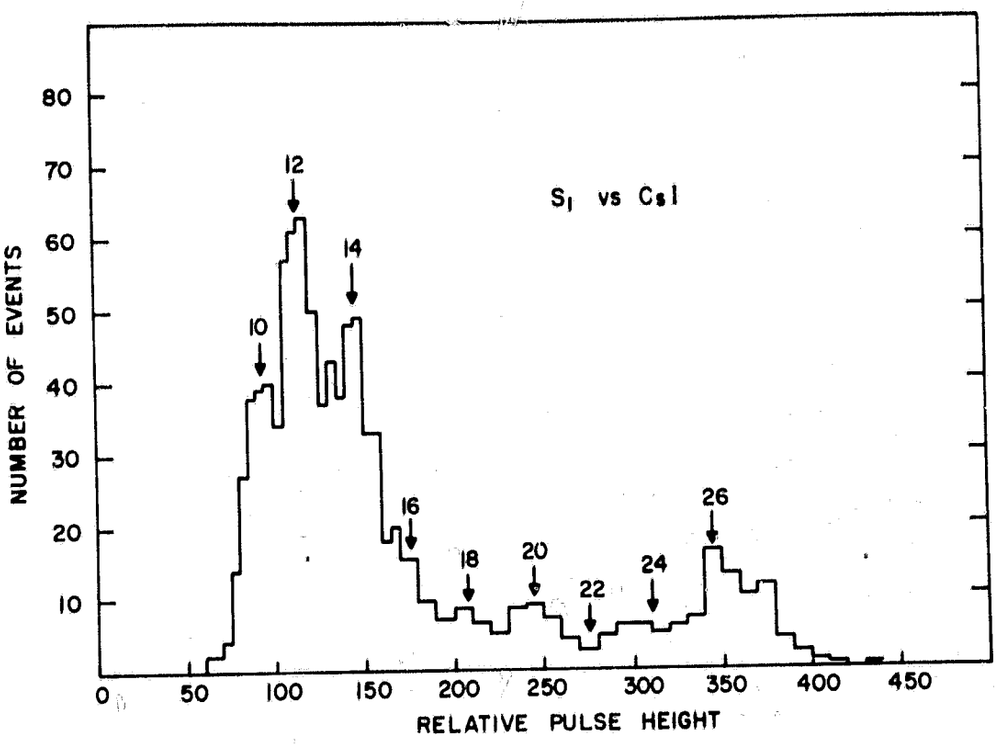
NUMBER OF EVENTS
RELATIVE PULSE HEIGHT
S1 vs CsI
10
12
14
16
18
20
22
24
26

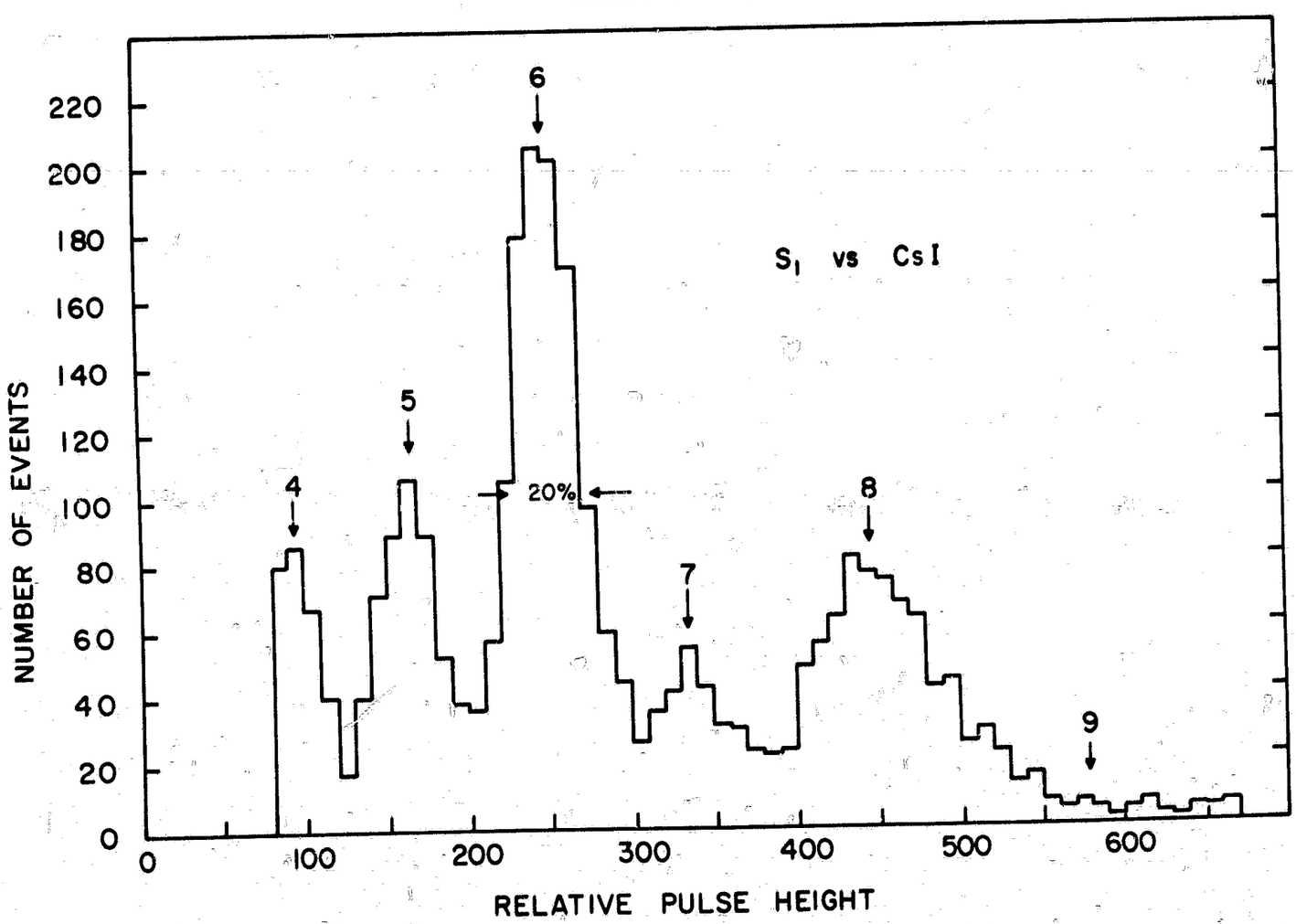
NUMBER OF EVENTS
RELATIVE PULSE HEIGHT
S1 vs CsI
4
5
6
7
8
9
20%